Unequal wave vectors in short- versus long-range ordering in intermetallic compounds

Z. W. Lu* and Alex Zunger
National Renewable Energy Laboratory, Golden, Colorado 80401
(Received 22 April 1994)

The sign of the formation energy ΔH_F of a compound indicates if the low-temperature long-range order (LRO) corresponds to compound formation (when $\Delta H_F < 0$) or to phase-separation (when $\Delta H_F > 0$). However, ΔH_F by itself does not tell us what type (ordering or clustering) of high-temperature short-range order (SRO) can be expected. The reason is that ΔH_F contains two *types* of contributions: an "elastic," volume-deformation energy $G(x)$ that reflects the energy invested in deforming the constituents A and B to the volume $V(x)$ of the $A_{1-x}B_x$ alloy, and a "chemical" energy ε that reflects A-B interactions (charge transfer and atomic relaxations) at a *fixed* $V(x)$. We show that the LRO and the SRO have the same behavior only when the signs of ΔH_F and ε are the same: ordering tendencies ("type I") when both $\Delta H_F < 0$ and $\varepsilon < 0$, or phase-separating/clustering tendencies ("type III") when both $\Delta H_F > 0$ and $\varepsilon > 0$. However, "type II" systems ($\Delta H_F > 0$; $\varepsilon < 0$) can exhibit a phase-separating LRO and an ordering-type SRO. Direct self-consistent local-density calculations of the total energy coupled with Monte-Carlo simulated annealing calculations of the ensuing Ising-like cluster expansion illustrate these type I, II, and III behaviors in Ni-V, Ni-Au, and Pd-Rh, respectively.

I. INTRODUCTION

The structural properties of intermetallic systems are manifested both through low-temperature long-range order (LRO) and by high-temperature short-range order (SRO) which are measured[1] by Bragg diffraction and diffuse scattering, respectively. In most cases LRO and SRO have the same underlying reciprocal-space symmetry, described in terms of composition waves of given wave vectors. For example, the classic system[2] $Cu_{0.5}Au_{0.5}$ crystallizes at low temperatures in the $L1_0$ LRO structure which can be described as a Cu/Au/Cu/Au... superlattice along the [001] direction. As this structure disorders at higher temperatures (> 680 K), the x-ray diffuse scattering[3,4] exhibits peaks with a $\langle 001\rangle$ wave vector, indicative of SRO with the same wave vector symmetry as LRO. Indeed, the coincidence of the wave vector symmetries of LRO and SRO is so prevalent in the experimental literature on intermetallic alloys[1,5,6] and in its standard theoretical interpretation (the Krivoglaz-Clapp-Moss[7,8] mean-field theory) that any reported exception[9,10] creates significant interest.[11] Such are the cases of Pd_3V and Pt_3V, where low-temperature LRO corresponds to a $\langle 1\frac{1}{2}0\rangle$ superlattice (the DO_{22} structure) while high-temperature SRO peaks at $\langle 001\rangle$ points. Solal *et al.*[11] argued that this unusual behavior signals the breakdown of mean-field theory, while more recently, Wolverton *et al.*[12] showed that if *electronic excitations* are included the stable LRO becomes a function of temperature; at the temperature where SRO is $\langle 001\rangle$ type, the corresponding ordered $L1_2$ structure ($\mathbf{k}_{\rm LRO} = \langle 001\rangle$) is actually lower in energy than the DO_{22} structure ($\mathbf{k}_{\rm LRO} = \langle 1\frac{1}{2}0\rangle$). In this paper, we wish to present a simpler case where the wave vectors of LRO and SRO are different, namely, systems where the global ground state corresponds to (incoherent) phase separation (i.e., $\mathbf{k}_{\rm LRO} = \langle 000\rangle$ composition wave), yet coherent SRO corresponds to ordering tendencies (e.g., a $\mathbf{k}_{\rm SRO} = \langle 001\rangle$ wave). This duality *does not* conflict with mean-field theory. We will show that it corresponds to physical systems which phase separate due to size-mismatch-induced volume-altering *"elastic"* energies, yet their constant volume *"chemical"* interactions (i.e., charge transfer and relaxation) favor ordering. We will contrast the case $\mathbf{k}_{\rm LRO} \neq \mathbf{k}_{\rm SRO}$ with the conventional[7,8] $\mathbf{k}_{\rm LRO} = \mathbf{k}_{\rm SRO}$ case. We describe here a quantitative model, based on first-principles local-density calculations, illustrating compound-forming (Ni-V), phase-separating (Pd-Rh), and mixed (Ni-Au) behaviors. In the first two cases, the wave vectors of LRO and SRO are identical: $\langle 1\frac{1}{2}0\rangle$ in Ni-V and $\langle 000\rangle$ in Pd-Rh, in good agreement with the experiment.[13] We predict that the third case (Ni-Au) should exhibit a phase-separating ground state ($\langle 000\rangle$ LRO) with ordering tendencies at higher temperatures ($\langle 00\zeta\rangle$ SRO). This situation is analogous to the case of bulk-grown zinc-blende semiconductor alloys which are known to phase separate at low temperatures,[14] but are predicted[15–17] to exhibit $\langle 1\frac{1}{2}0\rangle$ SRO tendencies at higher temperatures if coherency can be maintained.

II. CALCULATING SRO AND LRO

A. Cluster expansion: separation into volume-dependent and -independent terms

Short- and long-range order in binary $A_{1-x}B_x$ systems is generally interpreted in terms of spin-$\frac{1}{2}$ lattice models in which each lattice site i ($i = 1, ..., N$) is labeled by a spin variable $\hat{S}_i$, taking on the value $-1(+1)$ if site i is

 ©1994 The American Physical Society

occupied by atom $A(B)$. The excess energy $\Delta E(\sigma, V)$ of any of the 2^N configurations σ is

$$\Delta E(\sigma, V) = E(\sigma, V) - [(1-x)E_A(V_A) + xE_B(V_B)] \ . \tag{1}$$

Equation (1) depends on volume V and is defined with respect to the energies of equivalent amounts of pure solid A and B at their respective equilibrium volume V_A and V_B. Low-temperature LRO of a given lattice type is then interpreted as the configuration σ which gives the lowest $\Delta E(\sigma, V_\sigma)$ at the equilibrium volume V_σ. Since quantum-mechanical calculations of an astronomic (2^N) number of such configurational formation energies $\Delta H_F(\sigma) \equiv \Delta E(\sigma, V_\sigma)$ is prohibitive, one performs such a "ground state search" by expanding Eq. (1) in a finite Ising-like "cluster expansion" (CE)

$$\Delta E_{\rm CE}(\sigma, V) = \sum_f D_f J_f(V) \overline{\Pi}_f(\sigma) \ , \tag{2}$$

where $J_f(V)$ are volume-dependent interaction energies of basic lattice "figures" f (e.g., nearest-neighbor pairs, next-neighbor pairs, triangles, etc.), and the "lattice-averaged spin products" $\overline{\Pi}_f(\sigma)$ are the product over the figure f of the variables $\hat{S}_i$, averaged over all symmetry equivalent figures of the lattice. All of the terms on the right-hand side of Eq. (2) are trivially determined geometrical quantities, with the exception of J_f, the effective interaction energies. Since $\{\overline{\Pi}_f(\sigma)\}$ is a complete, orthonormal set of polynomials, the expansion Eq. (2) is exact,[18] if not truncated. In practice, one hopes that this series converges reasonably rapidly, and so only $\sim O(10)$ interactions are retained (the first few pair interactions, as well as many-body terms). If the series (2) converges after M terms, an equivalent number of interaction energies $\{J_f(V)\}$ can be obtained by mapping Eq. (2) on $\sim M$ values of quantum-mechanically calculated excess energies [Eq. (1)] for, e.g., simple periodic configurations of known $D_f\overline{\Pi}_f(\sigma)$ values.[19] Convergence is then examined by the ability of these M interaction energies to reproduce via Eq. (2) the quantum-mechanically calculated energies of *other* configurations. This approach has recently been reviewed.[20]

Once a useful cluster expansion (2) is established, the lowest-energy "ground state structures" can be obtained efficiently[21] without having to visit all 2^N possibilities. Such a ground state search involves two steps: first, finding the lowest-energy configuration at each *fixed composition* x (thus, approximately at a fixed volume), and second, finding the global *ground state* among all compositions. It is, therefore, useful to partition Eq. (2) accordingly. Equation (1) can be rewritten as

$$\begin{aligned}\Delta E(\sigma, V) = &\{(1-x)[E_A(V) - E_A(V_A)] \\ &+x[E_B(V) - E_B(V_B)]\} \\ &+\{E(\sigma, V) - [(1-x)E_A(V) + xE_B(V)]\} \ .\end{aligned} \tag{3}$$

The first term in the curly brackets is the "volume deformation" energy associated with "preparing" A and B by deforming them to their final volume $V = V(x)$, while the second term is the energy change associated with forming σ from $A + B$ at the *fixed volume*. This partitioning was discussed in detail in Refs. 15–17, 22–25. Its most useful form is the "ε-G" representation:[17,22] Ferreira *et al.*[22] and Wei *et al.*[17] have shown that if the equilibrium volumes $V_\sigma(x)$ depend primarily on the composition x (either linearly or nonlinearly) and only weakly on the configuration σ, then the variables σ and x of Eq. (2) can be rigorously separated as

$$\Delta \tilde{E}_{\rm CE}(\sigma, V) = G(x) + \sum_f D_f \mathcal{V}_f \overline{\Pi}_f(\sigma) \equiv G(x) + \varepsilon(\sigma) \ . \tag{4}$$

The physical meaning of the two terms is as follows.

(i) The first term $G(x) \geq 0$ is essentially the elastic energy necessary to hydrostatically deform the constituents $(1-x)A + xB$ from their equilibrium volumes V_A and V_B to the alloy volume $V(x)$. Since $G(x)$ is positive definite, it is not a "relaxation energy." This elastic energy $G(x)$ is calculated[17] from

$$G(x) = (1-x)\int yZ(y)dy + x\int (1-y)Z(y)dy, \tag{5}$$

where $Z(x)$ is selected so that $\Delta \tilde{E}_{\rm CE}(\sigma, V)$ [Eq. (4)] and $\Delta E(\sigma, V)$ [Eq. (3)] have the same value and the same two volume derivatives. A simple approximation is[17]

$$Z(x) = \frac{B}{V}(dV/dx)^2, \tag{6}$$

where B is the bulk modulus and V is the volume.

(ii) The second term of Eq. (4) describes "everything else," i.e., $\varepsilon(\sigma) \equiv \Delta E(\sigma, V) - G[V(x)]$. This is the energy change when A combines with B at the volume $V(x)$ to form the AB compound at the same volume. This term is labeled as "spin-flip energy" or "chemical energy." Since in calculating $\Delta E(\sigma, V)$ we permit full cell-internal and cell-external relaxation as well as charge self-consistency, the quantity $\varepsilon = \Delta E(\sigma, V) - G(x)$ includes charge transfer and (nonhydrostatic) atomic relaxations. While relaxation is always energy lowering, charge transfer at a fixed volume need not be. Thus, ε can be either negative or positive. The cluster expansion of ε gives the volume- and composition-*independent* "spin-flip" interaction energies $\mathcal{V}_f$ for figure f. These spin-flip energies thus correspond to a cluster expansion of the excess energy $\Delta E(\sigma, V)$ *after* the elastic energy $G[V(x)]$ has been subtracted from it. We refer to Ref. 17, Sec. IV B, for the description of how $G(x)$ and $\mathcal{V}_f$ are calculated from a set of quantum-mechanical excess total energies of the form of Eq. (1).

The important point to notice from representation (4) is that while the *global* ground state structure corresponds to the minimum of the *sum* of the two terms of Eq. (4), the *relative* stability of different structures at the same composition depends only on the chemical energy ε [since $G(x)$ is a constant at fixed x]. Another way of saying this is that the "ordering energy" $\delta E_{\rm ord}(\sigma)$, defined as the difference between the formation enthalpy $\Delta H_F(\sigma)$ of

an ordered configuration σ and the energy $\Delta H_{\rm mix}(x)$ of a random alloy at the same x, does not depend on $G(x)$. Denoting a configurational average for the random (R) state by angular brackets $\langle\ \rangle_R$ this results follows from

$$\Delta H_{\rm mix} = G(x) + \sum_f D_f \mathcal{V}_f \langle \overline{\Pi}_f \rangle_R = G(x) + \sum_f D_f \mathcal{V}_f (2x-1)^{k_f} \quad , \tag{7}$$

where $\langle \overline{\Pi} \rangle_R = (2x-1)^{k_f}$ and k_f is the number of vertices in figure f. Hence,

$$\delta E_{\rm ord}(\sigma) = \sum_f D_f \mathcal{V}_f [\overline{\Pi}_f(\sigma) - (2x-1)^{k_f}] = \varepsilon(\sigma) - \varepsilon(\text{random}) \tag{8}$$

is not affected by volume deformation.

The separation of variables in the two terms of Eq. (4) has a physical implication in cases where ground state LRO is determined *incoherently* (i.e., each phase adopting its own equilibrium V_σ), while SRO is determined *coherently* (all competing structures being constrained to a fixed composition). Table I shows the three basic situations that can be encountered: Type-I systems have a negative formation energy $\Delta H_F < 0$ (thus, an ordering-type LRO at low temperatures), and the dominant spin-flip energy is antiferromagnetic $\mathcal{V}_f > 0$ (thus, an ordering-type SRO at higher temperatures). This leads to $\varepsilon < 0$ and $\delta E_{\rm ord} < 0$. Type-I systems thus correspond to the usual "compound-forming" systems where the elastic energy is overwhelmed by attractive chemical interactions and LRO and SRO both have their composition modulation wave vector $\mathbf{k}$ *off* $\langle 000 \rangle$ [note, however, that $\mathbf{k}_{\rm SRO}$ and $\mathbf{k}_{\rm LRO}$ may differ, as in the case of Pd_3V (Ref. 11)]. Type-III systems are just the opposite, having $\Delta H_F > 0$ and ferromagnetic spin-flip energies, and so LRO and SRO both have the same phase-separating/clustering wave vector $\mathbf{k} = \langle 000 \rangle$. This discussion shows that one could have an intermediate case (type-II systems) where $\Delta H_F > 0$ because the elastic energy is large [$G(x) \gg 0$], yet the dominant spin-flip energies are antiferromagnetic ($\mathcal{V}_f > 0$; $\delta E_{\rm ord} < 0$).

Note that if we do not separate $G(x)$ from $\varepsilon(\sigma)$ but extract instead the effective cluster interactions from the sum $\Delta H_F = G + \varepsilon$, then for type-II systems we are bound to get ferromagnetic $J_f < 0$ leading to a pure $\mathbf{k} = 0$ type SRO. This is true whether we relax ΔH_F or not (since $\Delta H_F > 0$ for type-II systems). Thus, for type-II systems the interaction energies $\{J_f\}$ that describe the *total enthalpies* are not appropriate to describe coherent SRO. The only consistent method to describe SRO for type-II systems is to extract the effective cluster interactions from $\Delta E(\sigma, V)$ *after* the elastic energies have been subtracted. This corresponds to retaining only the second term of Eq. (3), i.e., considering σ, A, and B all at the same volume. For type-II systems this term is negative (Table IV), and so the interaction energies $\{\mathcal{V}_f\}$ extracted from it will be antiferromagnetic leading to an off-Γ peak in SRO.

We have previously shown[25,26] that a hypothetical, nonrelativistic description of Ni-Pt leads to type-II behavior and that most bulk-grown semiconductor alloys belong to this class (Refs. 15–17, 20, 22–24). Here we concentrate on demonstrating quantitatively these prototype behaviors on actual metallurgical systems identified in the last column of Table I.

We selected two systems whose LRO and SRO are known experimentally to correspond to ordering type (Ni-V) and phase-separating type (Pd-Rh). To illustrate a type-II behavior we select a chemically reactive atom pair (likely $\varepsilon < 0$) which nevertheless has a large size mismatch ($G \gg 0$). An example is the Ni-Au (Ref. 27 suggests that Ti-V may also be a type-II system).

B. Calculating the cluster expansion parameters

We have calculated the excess energy $\Delta E(\sigma, V)$ vs volume V for 8–12 ordered structures σ in Ni-Au, Pd-Rh, and Ni-V. We use the local-density approximation[28] (LDA) as implemented by the full-potential linearized augmented-plane-wave (LAPW) method.[29] At the equilibrium volume V_σ the excess energy $\Delta E(\sigma, V_\sigma) = \Delta H_{\rm direct}$. We use the Wigner form[30] of the exchange-correlation potential. The core states are treated fully relativistically while the valence states are treated scalar relativistically. The Brillouin zone integration is performed using 60–400 special $\mathbf{k}$ points[31] in the irreducible zone.

We minimize the total energy with respect to both cell-internal and cell-external atomic degrees of freedom, assuming $V(x) = (1-x)V_A + xV_B$. This relaxation leads to major changes in the interaction energy and atomic geometry. To test the importance of relaxation and the extent to which we describe it cor-

TABLE I. Classification of three types (I, II, and III) of alloy systems according to their elastic energy $G(x)$, spin-flip chemical energy ε (which includes charge transfer and sublattice relaxation), and their sum — the formation enthalpy ΔH_F [see Eq. (4)]. Type-I alloys are "ordering," and so LRO and SRO occur at the wave vectors $\mathbf{k} \neq 0$ ($\mathbf{k}_{\rm LRO}$ and $\mathbf{k}_{\rm SRO}$ need not be equal). Type-III systems are "phase separating," and so LRO and SRO occur at the same wave vector $\mathbf{k} = 0$. Type-II alloys have ordering type SRO ($\mathbf{k} \neq 0$), but phase-separating LRO ($\mathbf{k} = 0$).

Type	ΔH_F	$G(x)$	ε	LRO	SRO	Example
I	−	+	−	$\mathbf{k} \neq 0$	$\mathbf{k} \neq 0$	Ni-V
II	+	+	−	$\mathbf{k} = 0$	$\mathbf{k} \neq 0$	Ni-Au
III	+	+	+	$\mathbf{k} = 0$	$\mathbf{k} = 0$	Pd-Rh

rectly, we must consider *disordered alloys* for which measurements of relaxed interatomic distances exist. If one ignores relaxation altogether (e.g., as in the generalized perturbation method,[32] concentration wave,[33] tight-binding direct configurational averaging,[34] and the embedded cluster method[35]), or includes only hydrostatic-like volume deformations,[36–38] then the A—A, B—B, and A—B bond lengths in an $A_{1-x}B_x$ alloy end up being equal. This could be a severe approximation:[20] Both cell-external and cell-internal relaxations change the spin-flip energies $\{\mathcal{V}_f\}$ and the atomic positions. For example, measurements[39] on disordered Ni-Au show that these relaxations create three distinct bond lengths Ni—Ni, Ni—Au, and Au—Au and a distribution around each of them. We have calculated the alloy bond lengths by minimizing the elastic energy of a supercell whose sites are occupied by Ni and Au so as to mimic a larger supercell [i.e., using the concept of special quasirandom structures[40,41] (SQS's)]. This minimization can be done either by using an atomistic total energy expression (e.g., LDA) or by using continuum elasticity. We have previously shown[41–43] that the two approaches yield very similar results for lattice distortions even at the limit of short period superlattices. Since the SQS happens to be a superlattice along some orientation $\mathbf{G}$, we will calculate its equilibrium interlayer spacing $c_{\rm eq}$ along $\mathbf{G}$ as a function of the perpendicular lattice constant $a_\perp$ using continuum elasticity, i.e.,

$$c_{\rm eq}^{(i)}(a_\perp) = a_{\rm eq}^{(i)} - [2 - 3q^{(i)}(\mathbf{G})][a_\perp - a_{\rm eq}^{(i)}] \ . \qquad (9)$$

Here $a_{\rm eq}^{(i)}$ is the cubic lattice constant of material i, $q^{(i)}(\mathbf{G})$ is the "strain reduction factor" along $\mathbf{G}$ given by[41,44] $q(\mathbf{G}) = 1 - B/[C_{11} + \gamma(\mathbf{G})\Delta]$, where $\Delta = C_{44} - (C_{11} - C_{12})/2$ is the elastic anisotropy, B is the bulk modulus, C_{ij} are the elastic constants, and the orientation dependence is given by the geometric constant

$$\gamma(\mathbf{G}) = \frac{4(l^2m^2 + m^2n^2 + n^2l^2)}{(l^2 + m^2 + n^2)^2} \ . \qquad (10)$$

Here, l, m, and n are the Miller indices for the direction $\mathbf{G}$. Equations (9) and (10) predict very well $c_{\rm eq}^{(i)}$ $(a_\perp)$ as computed by LDA for short period superlattices.[41–43] While the elemental solids Ni and Au have the equilibrium lattice constants $a_{\rm eq}^{(i)}$, in the alloy environment these will expand and contract, respectively, to the alloy value $a_\perp = a(x)$. We then imagine a coherent layer of pure Ni (or Au) whose perpendicular lattice constant is constrained to equal $a(x)$, finding from Eqs. (9) and (10) the Ni-Ni (or Au-Au) interlayer distances along $\mathbf{G}$. We then layer these Ni and Au planes in the SQS, finding the corresponding Ni and Au atomic position so that the interlayer distances matches those obtained above. Using the experimental C_{ij} and $a^{(i)}$, we find that the average bond lengths and the distribution widths are 2.64 ± 0.08 Å, 2.70 ± 0.11 Å, and 2.77 ± 0.09 Å, for Ni—Ni, Ni—Au, and Au—Au, respectively, for $Ni_{0.5}Au_{0.5}$. These compare favorably with experimental extended x-ray absorption fine structure (EXAFS) values[39] of 2.66 ± 0.11 Å, 2.70 ± 0.09 Å, and 2.78 ± 0.06 Å, respectively.

The directly calculated formation enthalpies $\Delta H_{\rm direct}(\sigma)$ are collected in Table II. Table III gives more details for Ni-V, where both relaxed and unrelaxed calculations are reported. At this point all that can be said is that Pd-Rh and Ni-Au have $\Delta H_F > 0$ while Ni-V has $\Delta H_F < 0$, but with this information alone one cannot determine yet if Pd-Rh and Ni-Au are type-II or type-III systems.

Next, the directly calculated excess energies $\Delta E(\sigma, V)$ are mapped, as described in Ref. 17, onto $\Delta\tilde{E}_{\rm CE}(\sigma, V)$ of Eq. (4), thus obtaining $G(x)$ and the relaxed[45] $\{\mathcal{V}_f\}$. We use 8–12 figures described in Table IV which also gives the spin-flip energies $\mathcal{V}_f$, the chemical energy $\varepsilon(\sigma)$, and the elastic energy $G(x)$. The signs of Table I are corroborated. We see that the nearest pair interaction is the largest; however, the three- and four-body interactions (see, in particular, K_4) are quite substantial. We have predicted $\Delta H_{\rm CE}(\sigma)$ for the five structures that are *not* used in the fit. The resulting average prediction error is

TABLE II. Listing of the directly calculated, relaxed LAPW energies $\Delta H_{\rm direct}(\sigma)$ and the ε-G (Refs. 17, 22) cluster-expanded values $\Delta H_{\rm CE}(\sigma)$ for $A_{1-x}B_x$ in various structures defined in Table III. Here A = Pd and Ni, and B = Rh, Au, and V. Energy is in units of meV/atom. In the case of Ni-V, the ΔH are taken with respect to fcc Ni and bcc V, and so the energy zero is ΔH[Ni(fcc)] = 0.0 and ΔH[V(bcc)] = 0.0. However, $\Delta H_{\rm direct}$[V(fcc)] = 265.2 meV/atom.

	$Ni_{1-x}V_x$		$Ni_{1-x}Au_x$		$Pd_{1-x}Rh_x$	
Structure	$\Delta H_{\rm direct}(\sigma)$	$\Delta H_{\rm CE}(\sigma)$	$\Delta H_{\rm direct}(\sigma)$	$\Delta H_{\rm CE}(\sigma)$	$\Delta H_{\rm direct}(\sigma)$	$\Delta H_{\rm CE}(\sigma)$
fcc (A)	0.0	−13.0	0.0	0.0	0.0	1.3
$L1_2$ (A_3B)	−210.1	−211.0	75.5	75.5	66.8	72.4
DO_{22} (A_3B)	−315.2	−314.3			69.0	63.4
$\beta 1$ (A_2B)	−200.4	−231.5			72.5	59.6
$L1_0$ (AB)	−239.9	−194.6	76.8	76.8	82.4	88.6
$L1_1$ (AB)	−51.8	−37.8	167.6	167.6	79.0	79.0
"40" (A_2B_2)	−82.7	−94.2	83.8	83.8	70.7	70.5
$Z2$ (A_2B_2)	−159.5	−123.6	124.3	124.3	35.1	47.0
$\beta 2$ (AB_2)	−91.0	−94.5			64.2	59.2
DO_{22} (AB_3)	10.9	2.5			63.8	69.9
$L1_2$ (AB_3)	−2.9	−15.4	78.2	78.2	85.0	78.9
fcc (B)	265.2	273.9	0.0	0.0	0.0	−1.3

TABLE III. Listing of the LAPW-calculated unrelaxed and relaxed $\Delta H(\sigma)$ (in meV/atom) for $Ni_{1-x}V_x$ taken with respect to fcc Ni and bcc V. ΔH[Ni(fcc)] =0.0, ΔH[V(bcc)] = 0.0, and ΔH[V(fcc)] = 265.2 meV/atom. The ε-G cluster-expanded (CE) results (Refs. 17, 22) are also shown. Many of the structures calculated here can be characterized as a $(Ni)_p(V)_q$ superlattice in orientation $\hat{G}$. We use the conventional structure type name whenever available and assign an arbitrary name for other structure type. The structures marked with an asterisk are used in the CE fit.

Orientation	[001]	[011]	[012]	[111]	[113]
formula					
AB	$L1_0$*	$L1_0$*	$L1_0$*	$L1_1$*	$L1_1$*
Unrelaxed	−229.3	−229.3	−229.3	−50.2	−50.2
Relaxed	−239.9	−239.9	−239.9	−51.8	−51.8
CE	−194.7	−194.7	−194.7	−37.9	−37.9
A_2B	$\beta 1$*	$MoPt_2$*	$MoPt_2$*	$\alpha 1$*	$MoPt_2$*
Unrelaxed	−198.7	−301.9	−301.9	−90.2	−301.9
Relaxed	−200.4	−302.3	−302.3	−91.2	−302.3
CE	−231.0	−307.9	−307.9	−82.1	−307.9
AB_2	$\beta 2$	$MoPt_2$*	$MoPt_2$*	$\alpha 2$*	$MoPt_2$*
Unrelaxed	−91.0	27.6	27.6	93.7	27.6
Relaxed					
CE	−96.5	56.1	56.1	97.5	56.1
A_3B	$Z1$*	$Y1$*	DO_{22}*	$V1$*	$W1$*
Unrelaxed	−148.4	−230.4	−313.3	−74.0	−182.7
Relaxed	−153.6	−232.5	−315.2	−75.5	
CE	−162.3	−212.7	−314.3	−50.7	−215.4
AB_3	$Z3$*	$Y3$*	DO_{22}	$V3$	$W3$*
Unrelaxed	31.5	62.9	10.9	151.0	69.2
Relaxed					
CE	5.7	84.8	2.9	151.2	29.1
A_2B_2	$Z2$*	$Y2$*	"40"*	$V2$	$W2$*
Unrelaxed	−139.5	−67.0	−81.6	60.5	−124.6
Relaxed	−159.5		−82.7		
CE	−124.8	−96.0	−94.0	54.0	−140.0
		other structures			
	$L1_2$ (A_3B)*	$L1_2$ (AB_3)*	DO_{23} (A_6B_2)	Ni_8Nb (A_8B)*	
Unrelaxed	−210.1	−2.9	−280.7	−189.4	
Relaxed	−210.1	−2.9			
CE	−211.0	−15.6	−262.6	−175.5	

TABLE IV. Definition of the "figures" f used in our cluster expansion in terms of the vertices of the fcc structure (in units of $\frac{a}{2}$, where a is the lattice parameter). The effective $T = 0$ cluster interactions $\mathcal{V}_f$ (including the degeneracy factor D_F) are obtained in the ε-G representation for Ni-V, Pd-Rh, and Ni-Au. We also give the temperature-dependent (T = 1400 K) effective interaction values for Ni-V according to the prescription of Ref. 12. Negative (positive) $\mathcal{V}_f$ denote ferromagnetic (antiferromagnetic) interactions. We also give the values of α and β, which fit the elastic energy $G(x)$ to the form of $G(x) = 4[\alpha+\beta(x-\frac{1}{2})]x(1-x)$, and the calculated energy $\Delta H_{\rm mix}$ of completely random alloy at $x = \frac{1}{2}$ (corresponding to $T = \infty$). Note that $\Delta H_{\rm mix}(\frac{1}{2}) = \alpha + J_0$. In addition, the total chemical energy $\varepsilon(\sigma)$ is given for the $L1_0$ structure and the random alloy, as is the ordering energy $\Delta E_{\rm ord}(L1_0)$. All quantities are in units of meV/atom.

Cluster Type	Designation	Vertices	Ni-V		Ni-Au	Pd-Rh
			$T = 0$ K	$T = 1400$ K	$T = 0$ K	$T = 0$ K
Empty	J_0		−233.2	−233.2	−452.9	53.3
Point	J_1	(000)	252.9	252.9	39.0	2.3
Pairs	J_2	(000),(110)	152.0	152.0	217.9	−46.0
	K_2	(000),(200)	−20.0	−20.0	25.6	−0.1
	L_2	(000),(211)	58.9	58.9	157.2	−10.8
	M_2	(000),(220)	33.5	33.5	60.6	8.2
Triplets	J_3	(000),(110),(101)	−96.1	−142.7	−39.0	−3.6
	K_3	(000),(110),(200)	44.5	44.5		
	L_3	(000),(110),(211)	64.5	64.5		
	M_3	(000),(110),(002)	−41.1	−41.1		
	Q_3	(000),(110),(220)	−81.3	−81.3		
Quadruplets	J_4	(000),(110),(101),(011)			−8.4	−4.6
	K_4	(000),(110),(101),(200)	139.1	−35.6		
$G(x)$	α		141.9	141.9	579.5	12.9
	β		−30.2	−30.2	−208.9	1.5
$\Delta H_{\rm mix}(\frac{1}{2})$			−91.3		126.6	66.2
$G(\frac{1}{2})$			141.9		579.5	12.9
$\varepsilon(L1_0)$			−336.4		−502.7	69.5
ε(rand)			−233.2		−452.9	53.3
$\delta E_{\rm ord}(L1_0)$			−103.2		−49.8	16.2

9.6 meV/atom and the maximum prediction error is 18.1 meV/atom.

Having obtained the interaction energies $\{V_f\}$ and $G(x)$ (Table IV), we can easily calculate the energy $\Delta H_{\rm mix}(x)$ of completely random alloy (no SRO, i.e., at $T=\infty$) using Eq. (7). Table IV gives this $\Delta H_{\rm mix}(\frac{1}{2})$. As the temperature is lowered from $T=\infty$, we expect[17] $\Delta H_{\rm mix}$ to be reduced.

Now we can distinguish different behaviors in Pd-Rh and Ni-Au: Despite the fact that both systems are phase separating ($\Delta H_F > 0$), the dominant nearest pair interactions are *antiferromagnetic* in Ni-Au ($V_f > 0$) but ferromagnetic for Pd-Rh ($V_f < 0$). Thus, Pd-Rh and Ni-Au have $\Delta H_F > 0$ for fundamentally different reasons: In Ni-Au, $\Delta H_F > 0$ because of the dominance of the elastic energy $G(x)$ (noted also by Wu and Cohen[46]) over the antiferromagnetic chemical interactions, while in Pd-Rh $\Delta H_F > 0$ because the chemical interactions themselves are ferromagnetic (i.e., promote phase separation). Table IV further shows that both in type-I and type-II structures $\varepsilon(L1_0) < \varepsilon$(random) or $\delta E_{\rm ord} < 0$, while in type-III structures $\varepsilon(L1_0) > \varepsilon$(random) or $\delta E_{\rm ord} > 0$. This means that in type-I and -II structures some ordered phases (e.g., $L1_0$) have a lower energy than the random alloy of the same composition. Yet, in type-II structures, phase separation has the absolute lowest energy. This sequence of energies exists in most semiconductor alloys; SRO above the miscibility gap temperature is of the $\langle 1\frac{1}{2}0\rangle$ ordering type.[15–17,22–24]

C. Finding SRO and LRO from the cluster expansion

Having calculated the parameters of the Hamiltonian, Eq. (4), we subject it to a Monte Carlo–simulated annealing treatment,[47–50] which gives us the $T=0$ LRO ground states (on a finite cell) as well as the SRO diffuse scattering map at a fixed temperature.[45] A Monte Carlo cell size of $16^3 = 4096$ atoms (with periodic boundary conditions) was used in most calculations (in Ni_2V, cell size of 18^3 was also used). Monte Carlo–simulated annealing was performed in the canonical ensemble at a fixed concentration, with the transition temperature being calculated from the discontinuity in the internal energy as a function of temperature, and the ground state determined by the state of the simulation at a temperature where all configurational changes proved to be energetically unfavorable. Since we run the Monte Carlo simulation with decreasing temperature, it tends to supercool a structure. The resulting transition temperature is thus a lower bound of the real T_c. The estimated error is around 100 K.

The Warren-Cowley SRO parameter[51] for the Nth atomic shell at distance R from the origin is

$$\alpha_{\rm SRO}(N) = \frac{\langle \overline{\Pi}_{0,N}\rangle - q^2}{1-q^2} \ , \tag{11}$$

where $q = 2x-1$ and the angular brackets denote configurational average. Note that $\alpha_{\rm SRO}(0) \equiv 1$ by definition. The Fourier transform of real-space SRO is $\alpha_{\rm SRO}(\mathbf{k})$, which is proportional to the diffuse intensity due to SRO. Its value depends on the number of N_R of real-space shells used in the transform:

$$\alpha_{\rm SRO}(\mathbf{k}, N_R) = \sum_{N}^{N_R} \alpha_{\rm SRO}(N) e^{i\mathbf{k}\cdot\mathbf{R}} \ . \tag{12}$$

In the calculation of $\alpha_{\rm SRO}(N)$ and $\alpha_{\rm SRO}(\mathbf{k}, N_R)$, 500 Monte Carlo steps per site are used to equilibrate the system (which is initialized in a completely random state), and subsequently, averages are taken over 100 Monte Carlo steps per site. Twenty-one atomic shells ($N_R = 21$ or $R = 3a$ where a is the lattice parameter) of $\alpha_{\rm SRO}(N)$ are used in Eq. (12) to assemble $\alpha_{\rm SRO}(\mathbf{k}, N_R)$ for Pd-Rh and Ni-Au, whereas 35 and 10 shells are used for Ni_3V and Ni_2V, respectively. These latter two cases are dictated by the number of experimental SRO parameters reported.[13] Further details on our Monte Carlo simulated annealing calculations will be given in Ref. 50.

III. RESULTS

A. Ground state LRO

For both Pd-Rh and Ni-Au all ΔH_F values are positive, and so one expects a phase-separating ground state. Thus, no Monte Carlo–simulated annealing is needed. Since for Ni-Au the composition-independent chemical interactions $\{V_f\}$ are antiferromagnetic, it is interesting to conduct a ground state search using this set alone. This will produce *constant-volume* "ground states." This produces a rather complex structure with large unit cell at $x=\frac{1}{2}$; a reciprocal-space description of this structure shows a strong peak at $\mathbf{k} = \langle \frac{2}{3}00\rangle$. This structure is less stable than phase separation, but is more stable than the random alloy of the same composition.

For Ni-V, we correctly identify in our ground state search the observed[52] Pt_2Mo ($x=\frac{1}{3}$) and DO_{22} ($x=\frac{1}{4}$) structures as the ground states. The transition temperatures T_c (listed in Table V) are, however, overestimated. Since we only do Monte Carlo simulations with decreasing temperature, the T_c given here may be the lower bound the real T_c. Inclusion of electronic excitation effects[12,45] lowers for Ni_3V T_c from 1900 K to 1400 K at $x=\frac{1}{4}$, close to the measured result of 1318 K. Note that the calculated order-disorder transition temperature at Ni_3V is $\sim$ 50 K above that of Ni_2V of the same order as the experimental difference of 123 K. For $x=\frac{1}{9}$, the cluster expansion fails to find the experimentally observed Pt_8Ti-type structure as the ground state despite the fact that direct LAPW calculations find the Pt_8Ti-type structure to be the lowest-energy struc-

TABLE V. The calculated and experimental order-disorder transition temperatures T_c (in kelvin) for Ni_2V and Ni_3V. The experimental data are from Ref. 52.

T_c	Ni_2V	Ni_3V
Calc.	1850	1900
Expt.	1195	1318

ture at this composition. This reflects a fitting error in the cluster expansion: While LAPW gives a value of $\Delta H_{\text{direct}} = -189.4$ meV/atom the cluster expansion gives $\Delta H_{\text{CE}} = -175.5$ meV/atom. In fact, the cluster expansion places another structure lower in energy ($\Delta H_{\text{CE}} = -189.2$ meV/atom) than the Pt_8Ti structure. The LAPW-calculated $\Delta H_{\text{direct}} = -189.4$ meV/atom for the Pt_8Ti structure is actually ~ 50 meV/atom *below* the tie line connecting the known ground state DO_{22} at $x = \frac{1}{4}$ and end point $x = 0$. Thus, while LAPW predicts the Pt_8Ti-type structure to be the lowest-energy at $x = \frac{1}{9}$, the ~ 14 meV/atom error of the CE obscures this result in a ground state search.

B. Diffuse scattering SRO

Figure 1 gives the calculated diffuse scattering SRO [i.e., $\alpha(\mathbf{k}, N_R)$] for the three alloy systems studied. As described in Table I, Ni-V (type-I) shows peaks off-Γ, indicating ordering tendencies, and Pd-Rh (type-III) shows only Γ-like peaks, indicating phase-separating tendencies, while Ni-Au, which is predicted to phase separate in its ground state (Sec. III A), exhibits in SRO off-Γ structures, indicative of ordering tendencies.

In $Ni_{0.75}V_{0.25}$ the high-temperature diffuse scattering intensity peaks at $\mathbf{k} = \langle 1\frac{1}{2}0\rangle$ corresponding to the DO_{22} low-temperature ordered phase (the DO_{22} structure is a [210] superlattice). We have calculated the short-range order parameters at $T = 2300$ K (i.e., using $T/T_c = 1.21$) The calculated $\alpha(N)$ [Fig. 2(a)] and $\alpha(\mathbf{k}, N_R)$ (Fig. 3) capture the essence of the experiment[13] (performed just above the measured order-disorder transition temperature). The calculated and experimental peak intensities at $W = \langle 1\frac{1}{2}0\rangle$ are 8.5 and 4.2, respectively. Inclusion[12] of electronic excitation effects[45] reduce the calculated peak intensity to 4.1 (calculated at the same T/T_c ratio of 1.21).

While $Ni_{0.75}V_{0.25}$ exhibits the $W = \langle 1\frac{1}{2}0\rangle$ peak for both the low-temperature ordered structure and high-temperature short-range order, the observed[13] and calculated high-temperature SRO maps (Fig. 4) in $Ni_{0.667}V_{0.333}$ show peaks at the $W = \langle 1\frac{1}{2}0\rangle$ point rather than at the corresponding wave vector of the ordered low-temperature Pt_2Mo structure $\langle \frac{2}{3}\frac{2}{3}0\rangle$. This is due to the fact that it is impossible to build an A_2B structure with $\langle \frac{2}{3}\frac{2}{3}0\rangle$ waves alone. However, the Pt_2Mo is a rather versatile structure: It is a superlattice along a few directions [110], [210], and [311]. Hence its corresponding high-temperature diffuse intensity peak at $\langle 1\frac{1}{2}0\rangle$ is not surprising, as it is in the $\langle 1\frac{1}{2}0\rangle$ *family* of structures.[10] Indeed, our calculated SRO at $T = 2250$ K shows peaks at

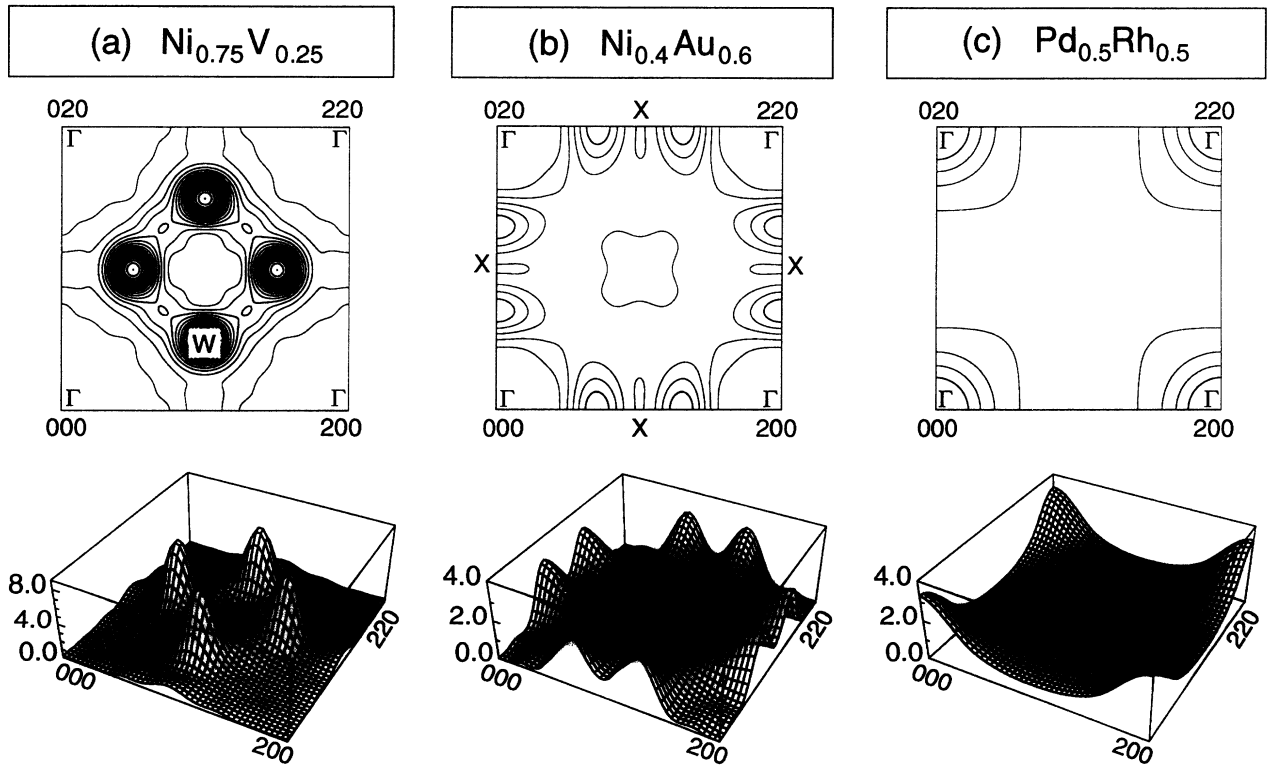

FIG. 1. Calculated SRO diffuse scattering map $\alpha(\mathbf{k}, N_R)$ [Eq. (12)] for (a) $Ni_{0.75}V_{0.25}$, (b) $Ni_{0.4}Au_{0.6}$, and (c) $Pd_{0.5}Rh_{0.5}$. The number of real-space atomic shells, N_R, used is $N_R = 35$ for Ni-V and 21 for Ni-Au and Pd-Rh. The Monte Carlo simulations were performed at $T = 2300$ K for $Ni_{0.75}V_{0.25}$ and 1500 K for Ni-Au and Pd-Rh. Note that the peaks are at the $W = \langle 1\frac{1}{2}0\rangle$ point in Ni-V, the Γ-X line in Ni-Au, and the Γ point in Pd-Rh. Electronic excitation effects (Ref. 45) are not included (see Ref. 12 for their effect).

$W = \langle 1\frac{1}{2}0\rangle$ points. Figures 2(b) and 4 compare the calculated and experimental $\alpha(N)$ and $\alpha(\mathbf{k}, N_R)$ ($N_R = 10$), where the experimental data were measured at $T = 1228$ K and the experimental results are scaled with respect to $\alpha_{\text{expt}}(0) = 0.825$. The calculated $\alpha(\mathbf{k}, N_R)$ agrees the experiment reasonably well. Quantitatively, the calculated and experimental peak intensities at $W = \langle 1\frac{1}{2}0\rangle$ are 3.4 and 3.3, respectively.

$Pd_{1-x}Rh_x$ is a prototypical phase-separating system (type-III). While Pd and Rh have a fairly small lattice mismatch of 2.3%, the repulsive chemical interaction between Pd and Rh drives them apart. Indeed, the $\alpha(\mathbf{k}, N_R)$ peaks at the Γ point as shown in Fig. 1(c). This behavior was also shown by Johnson *et al.*[53] using a Korringa-Kohn-Rostoker coherent ptoential approximation (KKR-CPA) method. There were a few previous theoretical attempts aimed at predicting the miscibility gap;[26,38,53,54] these include Connolly-Williams type,[26] direct configurational averaging,[38] and the mean-field CPA approaches.[53,54] The predicted miscibility gaps are generally overestimated by $\lesssim 400$ K with respect to experiment.[55]

Unlike Pd-Rh, the calculated SRO for $Ni_{0.4}Au_{0.6}$ $\alpha(\mathbf{k}, N_R)$ ($N_R = 21$) has a peak along the Γ-X $\langle h00\rangle$ line (rather than at the Γ point) as shown in Fig. 1, with peak position at $h_m \approx 0.8$. This is in agreement

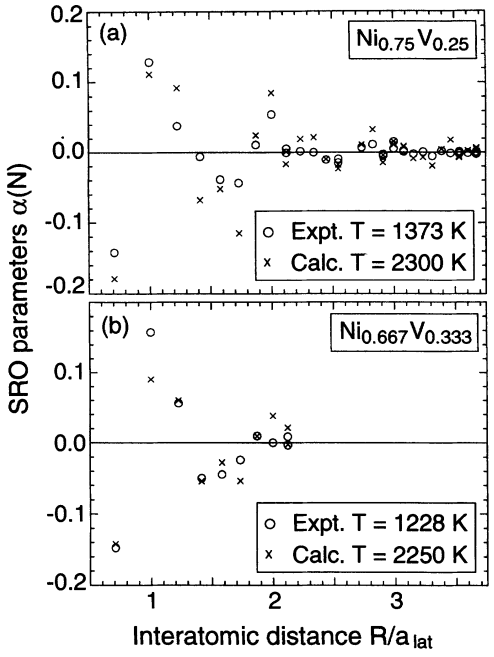

FIG. 2. Calculated and experimental (Ref. 13) real-space SRO parameters $\alpha(N)$ for (a) $Ni_{0.75}V_{0.25}$ and (b) $Ni_{0.667}V_{0.333}$.

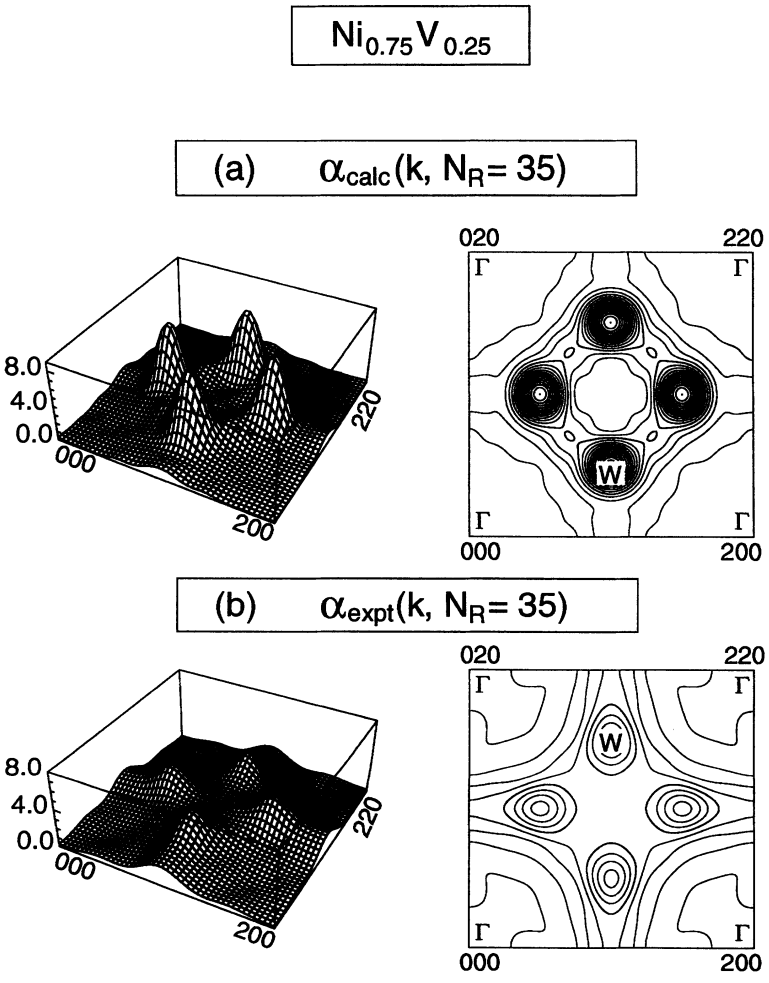

FIG. 3. Calculated and experimental [Ref. 13(b)] SRO diffuse scattering maps $\alpha(\mathbf{k}, N_R)$ ($N_R = 35$ pairs) for $Ni_{0.75}V_{0.25}$. The calculation was performed at $T = 2300$ K ($T/T_c = 1.21$), while the experimental data were measured at $T = 1373$ K ($T/T_c = 1.04$) just above the measured T_c. Note that Ref. 13(b) found from inverse Monte Carlo calculations $T_c^{\text{calc}} = 1113$ K and performed fits to the measured SRO at $T_{\text{SRO}}^{\text{calc}}/T_c^{\text{calc}} = 1.23$, close to our value of 1.21.

with an x-ray diffused scattering experiment by Wu and Cohen[56] on a $Ni_{0.4}Au_{0.6}$ single crystal at $T = 1023$ K. They observed that the measured short-range order intensity has a broad peak along the Γ-X ($\langle h00\rangle$) line, with maximum near $h_m \approx 0.6$. Our ε-only ground state search for $Ni_{0.5}Au_{0.5}$ (Sec. III A) did indeed produce a structure with a wave vector at $\mathbf{k} = \langle \frac{2}{3}00\rangle$. This point has the largest weight among all wave vectors for that structure. The calculated $\alpha(1) = -0.074$ has a different sign than the measured value of 0.039 of Wu and Cohen.[56] However, an earlier experiment[57] on $Ni_{1-x}Au_x$ film and polycrystalline samples suggested a negative $\alpha(1) \sim -0.030$ for $x = 0.6$. The calculated peak intensity of $\alpha_{SRO}(\mathbf{k})$, however, appears to be larger than experimental results of Wu and Cohen.[56] The competition between the chemical and elastic energies in Ni-Au has been discussed by de Fontaine and Cook[58] and by Wu and Cohen.[46] Using a phenomenological model developed by Cook and De Fontaine[59] and neutron inelastic as well as x-ray diffuse scattering data, Wu and Cohen[46] were able to correlate the minimum of the elastic energy in reciprocal space [$\langle h00\rangle$, $h = 0.6$] with the maximum in the experimental $\alpha_{SRO}(\mathbf{k})$.

It is interesting to note that while calculating *coherent* SRO [i.e., extracting $\mathcal{V}_f$ from the constant-volume energies $\varepsilon(\sigma)$] we find off-Γ peaks, calculating *incoherent* SRO [i.e., extracting J_f from excess enthalpies $\Delta H_F(\sigma) = G + \varepsilon(\sigma)$] gives SRO peaks only at the Γ point.

IV. SUMMARY AND CONCLUSIONS

We have shown that while the sign of the formation enthalpy, ΔH_F, is indicative of the type of low-temperature LRO (compound formation for $\Delta H_F < 0$; phase separation for $\Delta H_F > 0$), ΔH_F by itself does not tell us what type of SRO can be expected. However, the ε-G formalism[17,22] shows us how to decompose ΔH_F into an elastic volume-deformation (G) piece and a volume-independent chemical piece (ε). When $\varepsilon > 0$ we expect clustering-type SRO ($\mathbf{k} = \langle 000\rangle$), while $\varepsilon < 0$ indicates ordering-type SRO ($\mathbf{k}$ *off* $\langle 000\rangle$). In many cases SRO follows the wave vector symmetry of LRO, e.g., in "type-I" systems ($\Delta H_F < 0$; $\varepsilon < 0$) or in "type-III" systems ($\Delta H_F > 0$; $\varepsilon > 0$). We propose here "type-II" systems (Ni-Au and most bulk-grown III-V semiconductor alloys[15–17,22–24]), in which $\Delta H_F > 0$ due to the dominance of elastic energy ($G \gg 0$) over chemical ($\varepsilon < 0$) energies. In type-II systems the ground state is phase separating ($\Delta H_F = G + \varepsilon > 0$), yet at a fixed composition the *relative* energy of different structures shows ordering tendencies, and so the coherent $\mathbf{k}_{SRO}$ is *off* $\langle 000\rangle$.

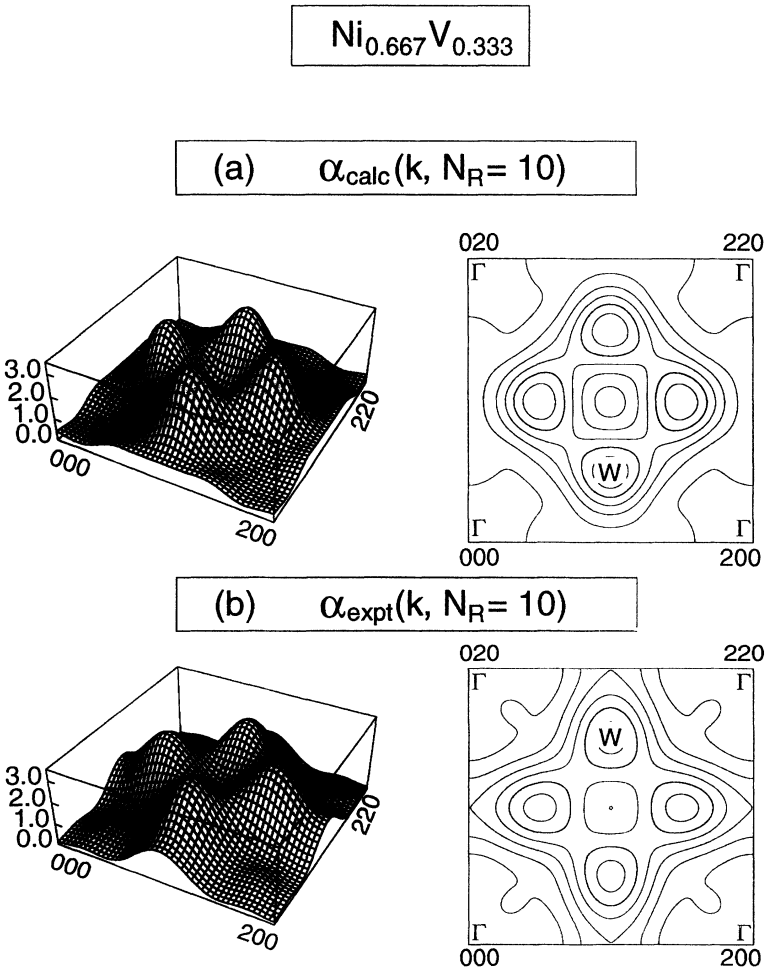

FIG. 4. Calculated and experimental (Ref. 13) SRO diffuse scattering maps $\alpha(\mathbf{k}, N_R)$ ($N_R = 10$ pairs) for $Ni_{0.667}V_{0.333}$. The calculation was performed at $T = 2250$ K ($T/T_c = 1.22$), while the experimental data was measured at $T = 1228$ K ($T/T_c = 1.03$) just above the measured T_c.

ACKNOWLEDGMENTS

Work at NREL was supported in part by the Office of Energy Research, Materials Science Division, U.S. DOE under Grant No. DE-AC02-83-CH10093. We thank Dr. Barry Klein and Dr. Christopher Wolverton for useful conversations.

---

* Present address: Department of Physics, University of California, Davis, CA 95616.

[1] B. E. Warren, *X-ray Diffraction* (Dover Publications, New York, 1990).

[2] *Phase Diagrams of Binary Gold Alloys*, edited by H. Okamoto and T. B. Massalski (ASM International, Materials Park, OH, 1987), p. 76.

[3] B. W. Roberts, Acta Metall. **2**, 597 (1954).

[4] E. Metcalfe and J. A. Leake, Acta Metall. **23**, 1135 (1975).

[5] W. Schweika, in *Statics and Dynamics of Alloy Phase Transformations*, edited by A. Gonis and P. E. A. Turchi, *NATO Advanced Study Institute, Series B: Physics* (Plenum Press, New York, 1994).

[6] L. Reinhard and S. C. Moss, Ultramicroscopy **52**, 223 (1993).

[7] M. A. Krivoglaz, *Theory of X-Ray and Thermal Neutron Scattering by Real Crystals* (Plenum, New York, 1969).

[8] P. C. Clapp and S. C. Moss, Phys. Rev. **142**, 418 (1966); *ibid* **171**, 754 (1968); S. C. Moss and P. C. Clapp, *ibid.* **171**, 764 (1968).

[9] There are two types of exceptions: when SRO and LRO belong to different "special points"(e.g., Pd_3V) or when SRO is at special points while LRO is not (e.g., Pt_2Mo); see Ref. 10. Here we discuss the former case; we thank D. de Fontaine for this clarification.

[10] D. de Fontaine, Acta Metall. **23**, 553 (1975).

[11] F. Solal, R. Caudron, F. Ducastelle, A. Finel, and A. Loiseau, Phys. Rev. Lett. **58**, 2245 (1987).

[12] C. Wolverton, A. Zunger, and Z. W. Lu, Phys. Rev. B **49**, 16 058 (1994).

[13] (a) R. Caudron, M. Sarfati, M. Barrachin, A. Finel, and F. Ducastelle, J. Phys. (France) I **2**, 1145 (1992); (b) A. Finel (private communication).

[14] M. B. Panish, in *Progress Solid State Chemistry*, edited by M. Reiss and J. O. McCaldin (Pergamon, New York, 1972), p. 39; K. Ishida, T. Shumiya, T. Nomura, H. Ohtani, and T. Nishizawa, J. Less. Common. Met. **142**, 135 (1988).

[15] L. G. Ferreira, S.-H. Wei, and A. Zunger, Phys. Rev. B **40**, 3197 (1989).

[16] J. E. Bernard, R. G. Dandrea, L. G. Ferreira, S. Froyen, S.-H. Wei, and A. Zunger, Appl. Phys. Lett. **56**, 731 (1990).

[17] S.-H. Wei, L. G. Ferreira, and A. Zunger, Phys. Rev. B **41**, 8240 (1990).

[18] J. M. Sanchez, F. Ducastelle, and D. Gratias, Physica A **128**, 334 (1984); J. M. Sanchez, Phys. Rev. B **48**, 14013 (1993).

[19] J. W. D. Connolly and A. R. Williams, Phys. Rev. B **27**, 5169 (1983).

[20] A. Zunger, in *Statistics and Dynamics of Alloy Phase Transitions*, edited by P. E. A. Turchi and A. Gonis, *NATO Advanced Study Institute, Series B: Physics* (Kluwer, Dordrecht, 1994), p. 361.

[21] J. Kanamori and Y. Kakehashi, J. Phys. (Paris) **38**, 274 (1977).

[22] L. G. Ferreira, A. A. Mbaye, and A. Zunger, Phys. Rev. B **37**, 10547 (1988); **35**, 6475 (1987).

[23] G. P. Srivastava, J. L. Martins, and A. Zunger, Phys. Rev. B **31**, 2561 (1985); **38**, 12694(E) (1988).

[24] J. E. Bernard, L. G. Ferreira, S.-H. Wei, and A. Zunger, Phys. Rev. B **38**, 6338 (1988).

[25] Z. W. Lu, S.-H. Wei, and A. Zunger, Europhys. Phys. Lett. **21**, 221 (1993).

[26] Z. W. Lu, S.-H. Wei, and A. Zunger, Phys. Rev. Lett. **66**, 1753 (1991); *ibid.* **68**, 1961 (1992).

[27] L. Reinhard and P. E. A. Turchi, Phys. Rev. Lett. **72**, 120 (1994).

[28] P. Hohenberg and W. Kohn, Phys. Rev. **136**, B864 (1964); W. Kohn and L. J. Sham, *ibid.* **140**, A1133 (1965).

[29] O. K. Andersen, Phys. Rev. B **12**, 3060 (1975); E. Wimmer, H. Krakauer, M. Weinert, and A. J. Freeman, *ibid.* **24**, 864 (1981); D. R. Hamann, Phys. Rev. Lett. **42**, 662 (1979); S.-H. Wei and H. Krakauer, *ibid.* **55**, 1200 (1985); S.-H. Wei, H. Krakauer, and M. Weinert, Phys. Rev. B **32**, 7792 (1985).

[30] E. Wigner, Phys. Rev. **46**, 1002 (1934).

[31] H. J. Monkhorst and J. D. Pack, Phys. Rev. B **13**, 5188 (1976).

[32] F. Ducastelle and F. Gautier, J. Phys. F **6**, 2039 (1976); G. Treglia, F. Ducastelle, and F. Gautier, *ibid.* **8**, 1437 (1977).

[33] B. L. Gyorffy and G. M. Stocks, Phys. Rev. Lett. **50**, 374 (1983); D. D. Johnson, D. M. Nicholson, F. J. Pinski, B. L. Gyorffy, and G. M. Stocks, *ibid.* **56**, 2088 (1986).

[34] H. Dreyssé, A. Berera, L. T. Wille, and D. de Fontaine, Phys. Rev. B **39**, 2442 (1989); C. Wolverton, G. Ceder, D. de Fontaine, and H. Dreyssé, *ibid.* **45**, 13105 (1992); **48**, 726 (1993).

[35] A. Gonis, W. H. Butler, and G. M. Stocks, Phys. Rev. Lett. **50**, 1482 (1983); A. Gonis, G. M. Stocks, W. H. Butler, and H. Winter, Phys. Rev. B **29**, 555 (1984).

[36] S.-H. Wei, A. A. Mbaye, L. G. Ferreira, and A. Zunger, Phys. Rev. B **36**, 4163 (1987).

[37] M. Sluiter, Phys. Rev. B **40**, 11215 (1989); **42**, 10460 (1990).

[38] C. Wolverton, D. de Fontaine, and H. Dreyssé, Phys. Rev. B **48**, 5766 (1993).

[39] G. Renaud, N. Motta, F. Lancon, and M. Belakhovsky, Phys. Rev. B **38**, 5944 (1988).

[40] A. Zunger, S.-H. Wei, L. G. Ferreira, and J. E. Bernard, Phys. Rev. Lett. **65**, 352 (1990); S.-H. Wei, L. G. Ferreira, J. E. Bernard, and A. Zunger, Phys. Rev. B **42**, 9622 (1990); S.-H. Wei and A. Zunger, *ibid.* **43**, 1662 (1991); Z. W. Lu, S.-H. Wei, and A. Zunger, *ibid.* **44**, 10470 (1991).

[41] Z. W. Lu, S.-H. Wei, and A. Zunger, Phys. Rev. B **44**, 3387 (1991); **45**, 10314 (1992).

[42] R. G. Dandrea, J. E. Bernard, S.-H. Wei, and A. Zunger, Phys. Rev. Lett. **64**, 36 (1990).

[43] J. E. Bernard and A. Zunger, Appl. Phys. Lett. (to be published).

[44] D. M. Wood and A. Zunger, Phys. Rev. B **40**, 4062 (1989).
[45] In this study we calculate $\Delta H_{\text{direct}}(\sigma)$ at $T = 0$ and thus the ensuing interaction energies $\{\mathcal{V}_f\}$ correspond to $T = 0$. In metals, however, excitation of electrons at finite T creates holes below the Fermi level and electrons above it, thus modifying the internal energy $\Delta H(\sigma, T)$ and creating a corresponding electronic (el) entropy ΔS_{el}. The temperature-dependent free energy $\Delta H_{\text{direct}}(\sigma, T) - T\Delta S_{\text{el}}(T)$ could be used to extract a set of *temperature-dependent* interactions energies $\{\mathcal{V}_f(T)\}$ in the same manner that we have used $\Delta H_{\text{direct}}(\sigma, T = 0)$ to extract $\{\mathcal{V}_f(T = 0)\}$. In most cases, the corrections due to electronic excitations are insignificant. If, however, there are two structures whose density of state at ε_F are extremely different, then electronic excitations can alter the relative stability of these structures. Wolverton *et al.* (Ref. 12) have recently shown that this is the case for the DO_{22} and $L1_2$ modification of Ni_3V and Pd_3V. Inclusion of electronic excitations resulted in significant temperature dependence of $\{\mathcal{V}_f\}$, an improvement in the calculated SRO and transition temperatures, and most importantly, it explained the occurrence of a $\langle 001 \rangle$-type SRO in Pd_3V as a consequence of the stabilization of the $L1_2$ structure at high-temperatures rather than as an exotic non-mean-field effect (Ref. 11). In the present study we use the $T = 0$ interaction energies since we are only interested in establishing trends in SRO behavior.
[46] T. B. Wu and J. B. Cohen, Acta Metall. **32**, 861 (1984).
[47] N. Metropolis *et al.*, J. Chem. Phys. **21**, 1087 (1953).
[48] K. Binder and D. W. Heermann, *Monte Carlo Simulations in Statistical Physics* (Springer-Verlag, Berlin, 1988).
[49] *The Monte Carlo Method in Condensed Matter Physics*, edited by K. Binder (Springer-Verlag, Berlin, 1992).
[50] Z.-W. Lu, D. B. Laks, S. H. Wei, and A. Zunger, Phys. Rev. B **50**, 6642 (1994).
[51] J. M. Cowley, J. Appl. Phys. **21**, 24 (1950).
[52] *Phase Diagrams of Binary Vanadium Alloys*, edited by J. F. Smith (ASM International, Materials Park, OH, 1989).
[53] D. D. Johnson, P. E. A Turchi, M. Sluiter, D. M. Nicholson, F. J. Pinski, and G. M. Stocks, in *Alloy Phase Stability and Design*, edited by G. M. Stocks, D. Pope, and A. Giamei, MRS Symposia Proceedings No. 186 (Materials Research Society, Pittsburgh, 1991), p. 21; B. L. Gyorffy, D. D. Johnson, F. J. Pinski, D. M. Nicholson, and G. M. Stocks, in *Alloy Phase Stability*, edited by G. M. Stocks and A. Gonis, Vol. 163 of *NATO Advanced Study Institute, Series B: Physics* (Kluwer, Dordrecht, 1989), p. 421.
[54] Y. Wang, J. S. Faulkner, and G. M. Stocks, Phys. Rev. Lett. **70**, 3287 (1993).
[55] E. Raub, H. Beeskow, and D. Menzel, Z. Metallkd. **50**, 428 (1959); J. E. Shield and R. K. Williams, Scr. Metall. **21**, 1475 (1987).
[56] T. B. Wu and J. B. Cohen, Acta Metall. **31**, 1929 (1983).
[57] P. A. Flinn, B. L. Averbach, and M. Cohen, Acta Metall. **1**, 664 (1953).
[58] D. de Fontaine and H. E. Cook, in *Critical Phenomena in Alloys and Superconductors*, edited by R. E. Mills, E. Ascher, and R. I. Jaffee (McGraw-Hill, New York, 1971); p. 257.
[59] H. E. Cook and D. de Fontaine, Acta Metall. **17**, 915 (1969).

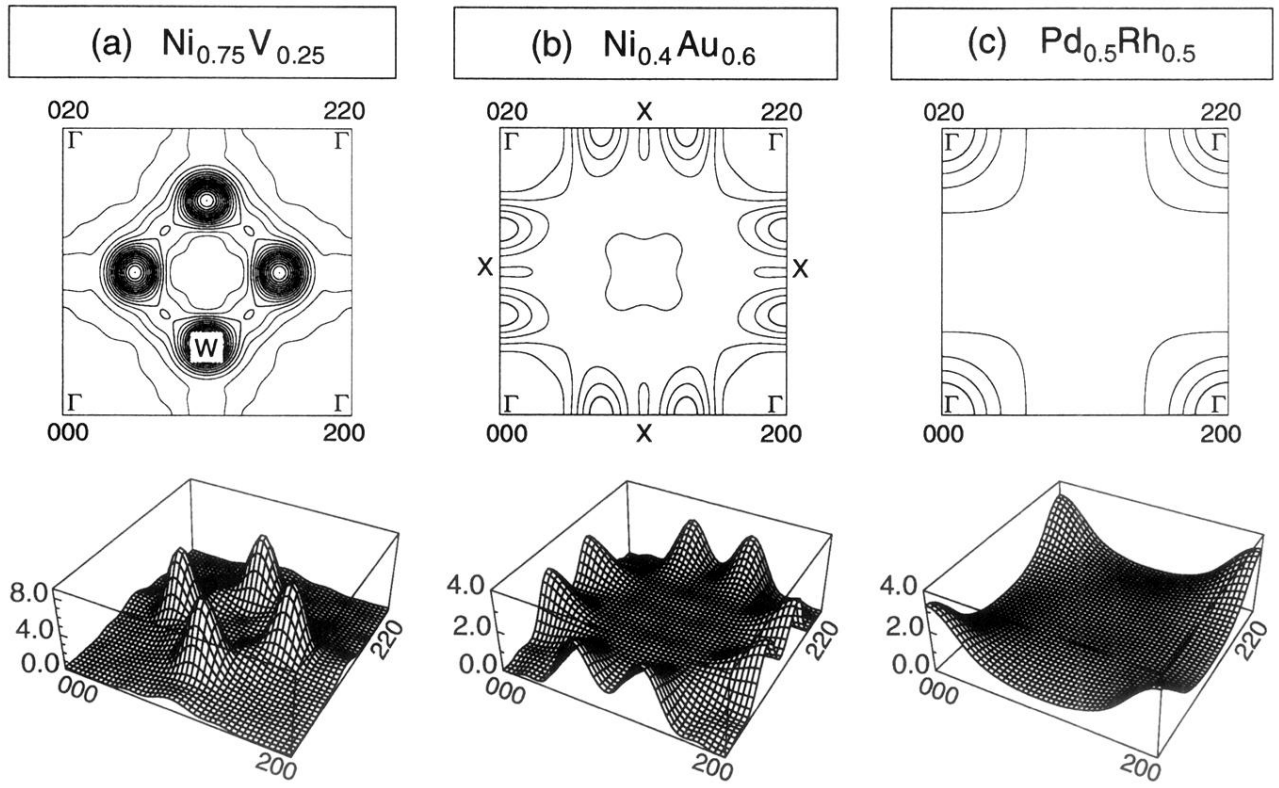

FIG. 1. Calculated SRO diffuse scattering map $\alpha(\mathbf{k}, N_R)$ [Eq. (12)] for (a) $Ni_{0.75}V_{0.25}$, (b) $Ni_{0.4}Au_{0.6}$, and (c) $Pd_{0.5}Rh_{0.5}$. The number of real-space atomic shells, N_R, used is $N_R = 35$ for Ni-V and 21 for Ni-Au and Pd-Rh. The Monte Carlo simulations were performed at $T = 2300$ K for $Ni_{0.75}V_{0.25}$ and 1500 K for Ni-Au and Pd-Rh. Note that the peaks are at the $W = \langle 1\frac{1}{2}0 \rangle$ point in Ni-V, the Γ-X line in Ni-Au, and the Γ point in Pd-Rh. Electronic excitation effects (Ref. 45) are not included (see Ref. 12 for their effect).

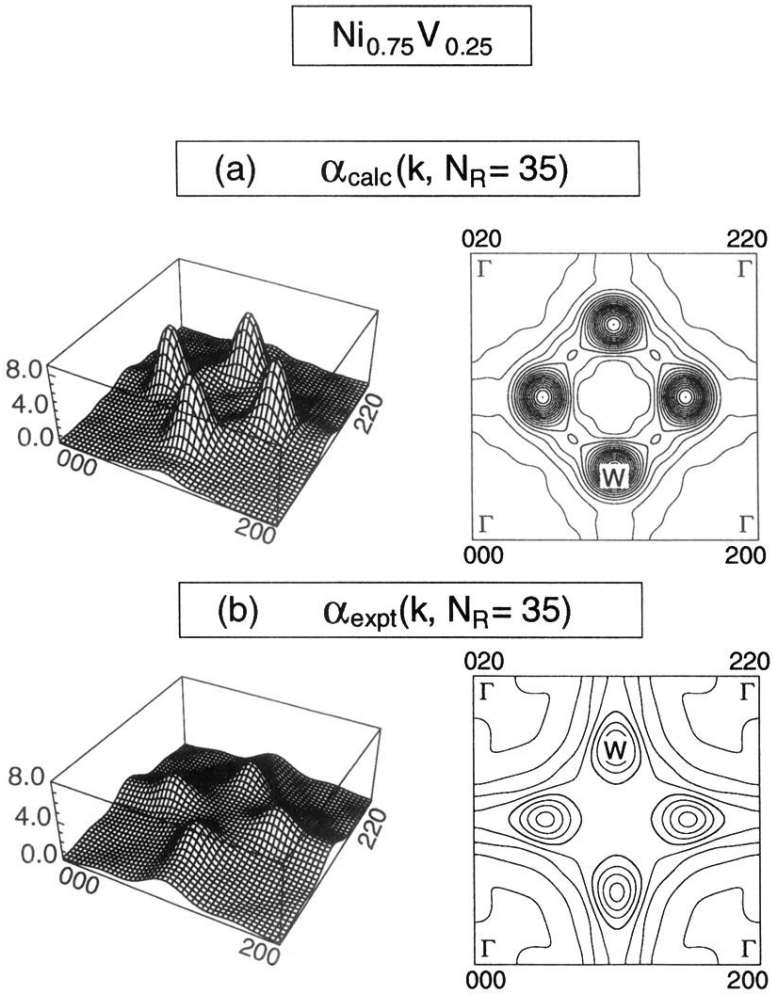

FIG. 3. Calculated and experimental [Ref. 13(b)] SRO diffuse scattering maps $\alpha(\mathbf{k}, N_R)$ (N_R = 35 pairs) for $Ni_{0.75}V_{0.25}$. The calculation was performed at T = 2300 K (T/T_c = 1.21), while the experimental data were measured at T = 1373 K (T/T_c = 1.04) just above the measured T_c. Note that Ref. 13(b) found from inverse Monte Carlo calculations $T_c^{\rm calc}$ = 1113 K and performed fits to the measured SRO at $T_{\rm SRO}^{\rm calc}/T_c^{\rm calc}$ = 1.23, close to our value of 1.21.

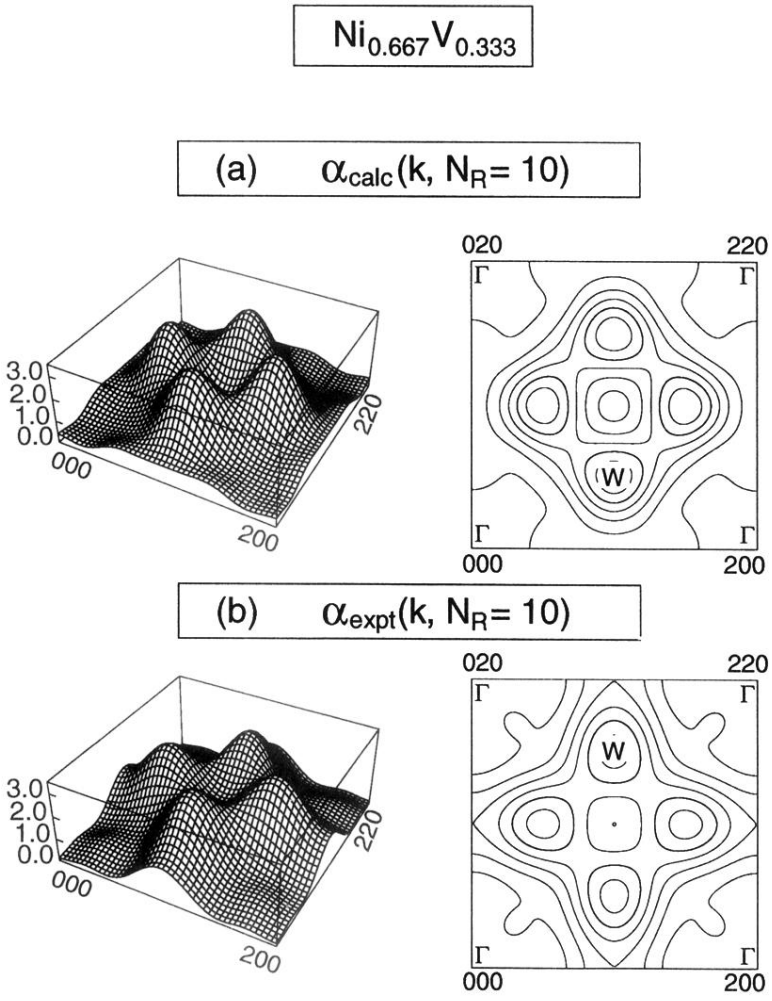

FIG. 4. Calculated and experimental (Ref. 13) SRO diffuse scattering maps $\alpha(\mathbf{k}, N_R)$ ($N_R = 10$ pairs) for $Ni_{0.667}V_{0.333}$. The calculation was performed at $T = 2250$ K ($T/T_c = 1.22$), while the experimental data was measured at $T = 1228$ K ($T/T_c = 1.03$) just above the measured T_c.